The Charge-Transfer Character of the $S_0 \rightarrow S_2$ Transition in the Carotenoid Peridinin Is Revealed by Stark Spectroscopy

Lavanya Premvardhan,*,†,# Emmanouil Papagiannakis,† Roger G. Hiller,‡ and Rienk van Grondelle†

Department of Biophysics and Physics of Complex Systems, Division of Physics and Astronomy, Faculty of Sciences, Vrije Universiteit, De Boelelaan 1081, 1081 HV Amsterdam, The Netherlands, and Macquarie University, New South Wales 2109, Australia

Received: April 19, 2005; In Final Form: June 3, 2005

Peridinin, the carotenoid in the peridinin chlorophyll *a* protein (PCP), was studied by Stark (electroabsorption) spectroscopy to determine the change in electrostatic properties produced on excitation within the absorption band, in methyl tetrahydrofuran (MeTHF) versus ethylene glycol (EG), at 77 K. Strikingly, a large change in the permanent dipole moment ($|\Delta\vec{\mu}|$) was found between the ground state, S_0 ($1^1A_g{}^{*-}$), and the Franck−Condon region of the S_2 ($1^1B_u{}^{*+}$) excited state, in both MeTHF (22 D) and EG (~27 D), thus revealing the previously unknown charge transfer (CT) character of this $\pi-\pi^*$ transition in peridinin. Such a large $|\Delta\vec{\mu}|$ produced on excitation, we suggest, facilitates the bending of the lactone moiety, toward which charge transfer occurs, and the subsequent formation of the previously identified intramolecular CT (ICT) state at lower energy. This unexpectedly large S_2 dipole moment, which has not been predicted even from high-level electronic structure calculations, is supported by calculating the shift of the peridinin absorption band as a function of solvent polarity, using the experimentally derived result. Overall, the photoinduced charge transfer uncovered here is expected to affect the excited-state reactivity of peridinin and, within the protein, be important for efficient energy transfer from the carotenoid S_2 and S_1/ICT states to the chlorophylls in PCP.

Introduction

The functional importance of carotenoids in photosynthesis is underscored by their ubiquitous presence as light harvestors and as photoprotectors that deactivate singlet oxygen and quench harmful triplets and radicals in plants.[1−3] A characterization of these systems is relevant to understand their effectiveness in photosynthesis and, furthermore, to design artificial systems[4,5] that mimic the useful properties that carotenoids exhibit in nature. Of the many carotenoids, peridinin (Scheme 1) is one of the most abundant and is found within the water-soluble peripheral peridinin chlorophyll *a* protein (PCP) and the membrane-associated intrinsic light-harvesting complex (LHC) of dinoflagellates.[6] Its primary role in energy transfer to chlorophyll *a* (Chl-*a*) in PCP[7−9] has led to extensive studies of its photophysics in the context of its biological function at the molecular level. Nevertheless, there remain unanswered questions about its electronic properties, particularly in the excited state. To this end, the Stark-effect study and solvent-shift analysis presented here provide new information about the electronic properties of the initially excited state, which complements the existing understanding of the rather peculiar photophysics of peridinin.[3,8,10−20]

The photophysical properties of carotenoids and retinals, decided by the nature of their potential energy surfaces (PES), are described in similar terms to (all-trans) linear polyenes of the C_{2h} point group because of the π-conjugated backbone they have in common.[21] The strongly allowed transition of carotenoids in the vis−near-UV wavelength region is characterized as a $1^1A_g{}^{*-} \rightarrow 1^1B_u{}^{*+}$ ($S_0 \rightarrow S_n$, most often $n = 2$) transition.[1] Absorption to S_1 ($2^1A_g{}^{*-}$), the lowest singlet excited state, is symmetry forbidden from the ground state and is thus not directly accessible by one-photon processes.[21] Although the PES of peridinin is described in a similar manner, it exhibits photophysical properties distinct from most other carotenoids. This has been attributed to the presence of a state, possibly S_1 itself, possessing charge-transfer (CT) character.[10,14,16,19,22] However, the identity and energetic location of this CT state, hereafter called the ICT state, continue to be strongly debated. Calculations find either a charge-transfer state distinct from S_1[14] or that S_1 itself possesses CT character.[16] Analysis of experimental studies also interpret the ICT state to be either strongly coupled to S_1[15,17] or distinct from S_1.[10,19] Of note is a recent multipulse transient absorption (pump−dump−probe) experi-

SCHEME 1: Molecular Structure of Peridinin[a]

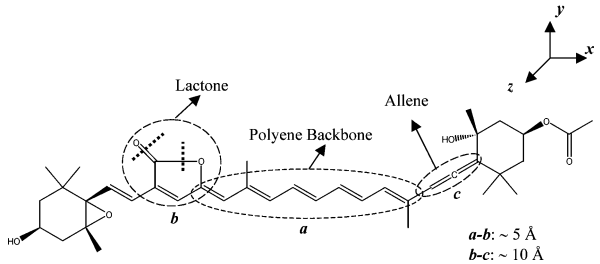

[a] The molecular structure of peridinin is shown with the different moieties encircled. The distances between the central points of these moieties are ~5 Å between *a* and *b* and ~10 Å between *b* and *c*. Also marked in the structure, in bold-dashed lines, are the nodes in the S_2 wave function[16] in the lactone ring (see text).

* To whom correspondence should be addressed. E-mail: lp2f@nat.vu.nl.
† Vrije Universiteit.
# Current Address: DBJC/SBFM, CEA-Saclay, Bât 528, 91191 Gif/Yvette, Cedex, France.
‡ Macquarie University.

10.1021/jp052027g CCC: $30.25
Published on Web 07/22/2005

ment,[19] which demonstrates that at early times after "dumping" the population of the ICT state, the S_1 population is not affected. Nevertheless, the equilibration of the S_1 and ICT states, after a few picoseconds, shows them to be coupled.

The importance of this charge-transfer state, energetically lower than S_2 (a $1^1B_u{}^{*+}$-like state), lies in its role as the major energy transfer funnel to Chl-*a* in PCP.[8,9] In that picture, the intrinsic electronic properties of S_2 are not invoked to explain the photophysics of peridinin, although >20% of energy transfer goes directly from S_2 to Chl-*a*.[8,9] The Stark-effect study presented here, from which the change in the electrostatic properties for the $S_0 \rightarrow S_2$ transition are obtained, and the accompanying solvatochromic analysis, however, suggest that the intrinsic polar nature of S_2 could be an important factor in effecting efficient energy transfer from peridinin in the protein. The effectiveness of the Stark study lies in being able to directly measure the change in the magnitude of the permanent dipole moment, $|\Delta\vec{\mu}|$, and the change in the electronic polarizability, $\overline{\Delta\alpha_{el}}$, from the field-induced change in the absorption spectrum.[23] In contrast to solvatochromic measurements at room temperature (RT), which are affected by thermal congestion, these properties can be deconvoluted in the Stark signal.[24] This experiment is particularly apt for peridinin because the presence of a CT state would be directly discernible, whether present as a unique entity or present within a manifold of overlapping states.

Notably, our experiments show that peridinin undergoes a large change in dipole moment,[25] typical of a charge-transfer transition, both in methyl tetrahydrofuran (MeTHF) and in ethylene glycol (EG), which may be directly attributed to the $S_0 \rightarrow S_2$ transition. Support for this rather surprising result, much greater than that predicted from other solvatochromic studies[10,12,17] and calculations,[16] is provided from the calculated shift of the electronic transition energy as a function of solvent polarity. The impact of this finding in peridinin is most relevant both for its biological functionality and to provide a benchmark for the performance of electronic-structure calculations. Future models of the excited-state PES of peridinin should take into account the polar character of S_2, expected to be important for enhancing the light-harvesting and energy-transfer capabilities of peridinin in PCP.

Materials and Methods

Peridinin was extracted from *Amphidinium carterae* thylakoids by the method of Martinson and Plumley[26] and was purified by reverse-phase HPLC using an Alltech C18 column.

Stark Experiment. Peridinin was dissolved in MeTHF (Aldrich) or EG (Aldrich) at room temperature, taking care not to expose the sample to ambient light. The ODs were between 0.3 and 0.5 in the sample cell at 77 K. MeTHF was refluxed for 1−2 h and redistilled, whereas EG (Sigma-Aldrich) was used directly. Double-sided sticking tape (~95 μm thick) and Kapton tape (~55 μm thick) were used as path length spacers for EG and MeTHF solutions, respectively. Magic angle measurements ($\chi = 54.7°$, eq 1) take into account the refractive indices of liquid nitrogen (LN2) and of MeTHF ($n = 1.79$)[27] or of EG ($n = 1.5$) at 77 K. The sample cell and apparatus are described in ref 28.

Analyzing the Stark Spectra. The Stark effect on the absorption spectrum, $A(\tilde{\nu})$, of an ensemble of molecules is determined from the difference in the intensity of the light transmitted through the sample in the presence of an external field. This change in the absorbance ($\Delta A(\tilde{\nu})$), or molar extinction coefficient, averaged over all orientations is analyzed using the Liptay expression:[23]

$$-\Delta A(\tilde{\nu}) = \vec{F}_{\text{eff}}{}^2\left[a_\chi A(\tilde{\nu}) + \frac{b_\chi \tilde{\nu}}{15h}\left\{\frac{\partial}{\partial\tilde{\nu}}\left(\frac{A(\tilde{\nu})}{\tilde{\nu}}\right)\right\} + \frac{c_\chi \tilde{\nu}}{30h^2}\left\{\frac{\partial^2}{\partial\tilde{\nu}^2}\left(\frac{A(\tilde{\nu})}{\tilde{\nu}}\right)\right\}\right] \quad (1)$$

$\Delta A(\tilde{\nu})$, a function of $\tilde{\nu}$, the energy in wavenumbers, is proportional to the square of the effective field, $\vec{F}_{\text{eff}}$, at the site of the solute and to the weighted sum of the (field-free) absorption line shape and the first and second derivative functions of $A(\tilde{\nu})$. (The first, second, and third terms in eq 1 are referred to as A′, B′ and C′, respectively, elsewhere in the text.) Experimentally, the change in transmitted light intensity due to the application of an electric field is measured and normalized by the total light intensity reaching the detector.[23] The coefficients of the derivatives of $A(\tilde{\nu})$ are related to $|\Delta\vec{\mu}|$ and $\overline{\Delta\alpha_{el}}$, the electrostatic properties of interest. When, χ, the angle between the applied AC electric-field vector and the electric-field vector of the polarized light, is set at the magic angle (54.7°), the expressions for the coefficients are

$$a_{54.7} = \frac{1}{30|\vec{m}|^2}\sum_{ij}[10A_{ij}{}^2] + \frac{1}{15|\vec{m}|^2}\sum_{ij}[10B_{ijj}] \quad (2)$$

$$b_{54.7} = \frac{1}{|\vec{m}|^2}\sum_{ij}[10m_iA_{ij}\Delta\mu_j] + \frac{15}{2}\overline{\Delta\alpha_{el}} \quad (3)$$

$$c_{54.7} = 5|\Delta\vec{\mu}|^2 \quad (4)$$

The coefficient a_χ (eq 1) is related to the electric-field induced change in the transition moment, $\vec{m}$: $\vec{m}(\vec{F}_{\text{eff}}) = \vec{m} + \underline{\mathbf{A}}\cdot\vec{F}_{\text{eff}} + \vec{F}_{\text{eff}}\cdot\underline{\underline{\mathbf{B}}}\cdot\vec{F}_{\text{eff}}$, where the tensors $\underline{\mathbf{A}}$ and $\underline{\underline{\mathbf{B}}}$ are the transition-moment polarizability and hyperpolarizability tensors, respectively. The $a_{54.7}$ component (eq 2) is usually very small compared to $b_{54.7}$ and $c_{54.7}$. A_{ij} can in theory be obtained from a_χ by measuring the Stark signal at various χ angles; however, in practice it is beset by a high degree of inaccuracy associated with extracting this parameter from the fit. The first-derivative coefficient, $b_{54.7}$, contains a component that is proportional to the second-rank tensor, $\underline{\underline{\Delta\alpha_{el}}}$, the difference electronic polarizability. In eq 3, $b_{54.7}$ is expressed in terms of the scalar quantity $\overline{\Delta\alpha_{el}}$ equal to $^1/_3\text{Tr}(\underline{\Delta\alpha_{el}})$, the average change in electronic polarizability between the ground and excited state. An accurate expression for $b_{54.7}$ includes an additional cross term comprising the tensor element of $\underline{\mathbf{A}}$, which is often neglected to be able to obtain $\overline{\Delta\alpha_{el}}$ directly from $b_{54.7}$.[29−33] This assumption, as shown in more modern and accurate formulations of the Liptay equation,[34] may however be erroneous, particularly if $|\Delta\vec{\mu}|$ is large, which is indeed the case for CT transitions. Therefore the experimental electro-optical parameter extracted from $b_{54.7}$, when A_{ij} is presumed to be negligible, will be reported as $\overline{\Delta\alpha^{\text{Stark}}}$, as in ref 35. When this assumption is erroneous, A_{ij} contributes to $\overline{\Delta\alpha^{\text{Stark}}}$ as follows: $\overline{\Delta\alpha^{\text{Stark}}} = \overline{\Delta\alpha_{el}} + (2/(15|\vec{m}|^2))\sum_{ij}[10m_iA_{ij}\Delta\mu_j]$. Although this quantity incorporates a polarizability symbol, the reader should keep in mind that $\overline{\Delta\alpha^{\text{Stark}}}$ is only proportional to one of two components that contains $\overline{\Delta\alpha_{el}}$, and is used here for historical reasons, albeit that it may be misleading. The expression for the coefficient of the second derivative at $\chi = 54.7°$ is directly proportional to the square of the change in permanent dipole moment, $|\Delta\vec{\mu}|$, as

TABLE 1: Electrostatic Properties of Peridinin[a]

	MeTHF	EG[b]
$\tilde{\nu}_{max}$ (λ_{max}), 298 K	21 620 (462.5)	20 750 (482)
$\tilde{\nu}_{max}$ (λ_{max}), 77 K	20 600 (485.5)	20 725 (482.5)
$\lvert\overline{\Delta\vec{\mu}}\rvert$ (D/f_c)	22 ± 3	27 ± 2
$\overline{\Delta\alpha}^{Stark}$ (Å^3/f_c^2)	−260 ± 170	−125 ± 100
$\lvert\hat{m}\cdot\Delta\vec{\mu}\rvert/\lvert\Delta\vec{\mu}\rvert$	0.98 ± 0.13	
$\Delta\alpha_m^{Stark}$ (Å^3/f_c^2)	−900 ± 300	

[a] The absorption maxima, $\tilde{\nu}_{max}$, are reported in wavenumbers (cm^{-1}) and in nm in parentheses (λ_{max}). The experimental values of $\lvert\Delta\vec{\mu}\rvert$ and $\overline{\Delta\alpha}^{Stark}$ are the electrostatic parameters, between S_0 and S_2, in MeTHF (methyl tetrahydrofuran) and EG (ethylene glycol). $\lvert\Delta\vec{\mu}\rvert$ includes an enhancement due to the local field, f_c, and $\overline{\Delta\alpha}^{Stark}$ to f_c^2 (see Materials and Methods). The ratio $\lvert\hat{m}\cdot\Delta\vec{\mu}\rvert/\lvert\Delta\vec{\mu}\rvert$ gives the cosine of the angle between $\lvert\Delta\vec{\mu}\rvert$ and $\hat{m}$, the unit vector in the direction of the transition moment. [b] The electrostatic properties in EG are reported from the fit to the absorption spectrum (Figure 2b). The outcome of the two-band fit (Figure 2c) is discussed in the text.

shown in eq 4. Note however that only the *magnitude* and not the sign of $\Delta\mu$ can be determined from the Stark signal, because the Liptay analysis follows from the assumption that the molecules in the sample are frozen in an isotropic orientation, both in the presence and absence of the external field.

In addition, the Stark spectrum at $\chi = 90°$ in conjunction with magic angle measurements yields values for $\lvert\hat{m}\cdot\Delta\vec{\mu}\rvert$, the magnitude of $\lvert\Delta\vec{\mu}\rvert$ along the transition dipole moment $\hat{m}$, and $\Delta\alpha_m$, a measure for the anisotropy in $\overline{\Delta\alpha}_{el}$, as shown:

$$\Delta\alpha_m = \frac{12b_{54.7} - 10b_{90}}{15} \tag{5}$$

$$\lvert\hat{m}\cdot\Delta\vec{\mu}\rvert = \sqrt{\frac{6c_{54.7} - 5c_{90}}{15}} \tag{6}$$

The expression for the change in polarizabilty along the transition moment, $\Delta\alpha_m$, in eq 5 assumes that the transition moment polarizability and hyperpolarizability contributions are negligible, and is therefore labeled as $\overline{\Delta\alpha}^{Stark}$ to make this distinction. We note that to obtain accurate values of $\lvert\hat{m}\cdot\Delta\vec{\mu}\rvert$ and $\Delta\alpha_m$, the fits to the Stark spectra at *both* $\chi = 54.7°$ and 90° must be good, which is the case here in MeTHF but not in EG. Therefore $\lvert\hat{m}\cdot\Delta\vec{\mu}\rvert$ and $\Delta\alpha_m$ are reported only for peridinin in MeTHF. In contrast, the fits in EG, even at $\chi = 54.7°$, are of much lower quality, so the absorption is deconvolved into Gaussians. The Stark spectrum is then fit to two bands, each composed of a sum of two or more of these Gaussians. This leads to an improved fit, suggesting that these bands correspond to electronic or vibronic transitions, underlying the absorption band, having unique electro-optical properties ($\lvert\Delta\vec{\mu}\rvert$ and $\overline{\Delta\alpha}_{el}$).[23] A detailed explanation of the procedure and the concomitant advantages and problems associated with such a fitting procedure are given in refs 34 and 36.

The coefficients of the derivatives, a_χ, b_χ, and c_χ, are extracted by means of a linear least-squares (LLSQ) fit of the electroabsorption signal to the sum of $A(\tilde{\nu})$ and the first and second derivatives of $A(\tilde{\nu})$. Smooth derivative functions are generated by first fitting the absorption spectra to a sum of Gaussians using a simplex algorithm.[36] It is adequate to smooth the Stark spectra with a polynomial filtering function or a sliding-average mean method, or both. The values of $\overline{\Delta\alpha}^{Stark}$ and $\lvert\Delta\vec{\mu}\rvert$, uncorrected by the cavity-field factor, f_c,[23] reported in Table 1, are the average of a minimum of three independent measurements. The effective field, $\vec{F}_{eff}$, arises from the enhancement of the external field due to the polarization of the solvent, such that $\vec{F}_{eff} = f_c \times \vec{F}_{ext}$, and $\vec{F}_{ext}$ is the external applied field. It is difficult to quantitate the effect of f_c on the Stark signal, particularly for a molecule such as peridinin where an accurate representation for the molecular cavity would be ellipsoidal. Therefore, this correction has not been made, and the experimental values of $\overline{\Delta\alpha}^{Stark}$ and $\lvert\Delta\vec{\mu}\rvert$ are reported in units of Å^3/f_c^2 and D/f_c (Table 1) and are likely to be 10−30% larger than the corresponding "unsolvated" gas-phase values. The f_c factors have been omitted for convenience but should be presumed present when referring to the experimental parameters throughout the text. The values for the peaks in the absorption spectra reported in Table 2, and referred to in the text, are obtained from the maxima of the second derivative function of the absorption line shape.

Calculating Solvent Shifts. The solvent shift between the condensed phase, $h\nu_{ab}$, and the gas phase, $h\nu_0$, can be estimated from dipole reorganization energies by treating the solvent as a dielectric continuum.[37] The solvent shifts depend on the reaction field factors, R_{or} and R_{el}, which arise from orientational and electronic effects, respectively, where the (total) reaction field factor at equilibrium, R_{eq} equals $R_{or} + R_{el}$. The reaction field factors for a polarizable point dipole along the, ith axis are[37]

$$R_{eq}^i = \frac{3}{a_x a_y a_z} A_i(1 - A_i)\frac{(\epsilon_0 - 1)}{\epsilon_0 + A_i(1 - \epsilon_0)} \quad \text{and}$$

$$R_{el}^i = \frac{3}{a_x a_y a_z} A_i(1 - A_i)\frac{(\epsilon_\infty - 1)}{\epsilon_\infty + A_i(1 - \epsilon_\infty)} \tag{7}$$

where ϵ_0 is the static dielectric constant and ϵ_∞ ($n^2 \approx \epsilon_\infty$) the

TABLE 2: Solvent Shift Analysis at 298 K[a]

	n-hexane	cyclohexane	MeTHF	THF	benzonitrile	acetonitrile
refractive index	1.37	1.42	1.41	1.40	1.53	1.34
ϵ_0, static dielectric	1.9	2.0	5.4	7.6	25.2	35.9
ν_{max} (expt)[b]	21990	21750	21620	21600	21000	21180
$h\Delta\nu^{exp}$	0	−240	−370	−390	−990	−810
$\mu_g = 6$ D, $\bar{\alpha}_g = 126$ Å^3, and $\Delta\mu = 2$; $\overline{\Delta\alpha} = 179$ Å^3 (ref 16)						
sphere $h\Delta\nu_{calc}$	0	−2	−12	−15	−21	−18
ellipse $h\Delta\nu_{calc}$	0	−4	−69	−82	−106	−109
$\mu_g = 6$ D, $\bar{\alpha}_g = 127$ Å^3, and $\Delta\mu = 18$; $\overline{\Delta\alpha} = 179$ Å^3						
sphere $h\Delta\nu_{calc}$	0	−116	−185	−182	−501	−92
ellipse $h\Delta\nu_{calc}$	0	−34	−487	−572	−724	−745

[a] The refractive index, n, and static dielectric constant, ϵ_0, used in eq 7 are given. The solvation energies, calculated using the gas-phase electrostatic properties,[16] are reported relative to the solvation shift in *n*-hexane, $h\Delta\nu_{calc}$, to be compared to the experimental shifts, $h\Delta\nu^{exp}$. The ground- and excited-state dipole moments, μ, and polarizabilities, $\bar{\alpha}$,[39] are taken from ref 16, except for the 18 D $\Delta\mu$ (see text). All energies are reported in wavenumbers (cm^{-1}). [b] The experimental values for the absorption maxima ν_{max} are taken from ref 10, except for that of MeTHF.

high-frequency dielectric constant. A_i accounts for the shape factor of the ellipsoidal cavity used for peridinin, which depend on the semi-axes of the ellipsoid, a_x, a_y, and a_z.[37] Here, a_x = 13 Å and $a_y = a_z = 2.5$ Å, which includes a 1 Å augmentation to account for the van der Waals radii along the *x*, *y*, and *z* directions (Scheme 1). In a spherical cavity, $a_x = a_y = a_z$, and is set here to be 13 Å to accommodate the long axis of peridinin.

The solvent shift, $h\nu_{ab} - h\nu_0$, between the absorption frequency in solution, ν_{ab}, and in vacuo, ν_0, with the solute modeled as a polarizable point dipole in the center of an ellipsoidal or a spherical cavity is calculated using the formulation by Kim:[38]

$$h\nu_{ab} - h\nu_0 = -R_{or}(\vec{\mu}_e - \vec{\mu}_g)\cdot\vec{\mu}_g - \frac{1}{2}R_{el}(\mu_e^2 - \mu_g^2) - \frac{1}{8}\bar{\bar{\alpha}}R_{el}^2(\mu_e^2 - \mu_g^2) + \frac{1}{2}\overline{\Delta\alpha}R_{or}^2\vec{\mu}_e\cdot\vec{\mu}_g - \frac{1}{2}\overline{\Delta\alpha}R_{or}(2R_{or} + R_{el})\mu_g^2 - \frac{1}{16}\overline{\Delta\alpha}R_{el}^2(\mu_e^2 - \mu_g^2) - R_{or}\bar{\bar{\alpha}}R_{eq}(\vec{\mu}_e - \vec{\mu}_g)\cdot\vec{\mu}_g \quad (8)$$

Here, $\bar{\bar{\alpha}} \cong {}^1/_2(\bar{\alpha}_g + \bar{\alpha}_e)$ and the ground- and excited-state components are labeled with subscripts "g" and "e", respectively.

In contrast to the Onsager or Lorenz model,[37] this formulation is exact to first order in polarizability. Note that the (sum of the) first two terms in eq 8 corresponds to the free energy cost for polarizing the medium (the self-energy) to equilibrate to the solute dipole. For an electronic transition in the condensed phase, the solvent field arising from both the orientational and electronic polarization is equilibrated with the *ground-state* dipole moment. In the Franck−Condon region, only the electronic polarization component, arising from the high-frequency dielectric, is able to follow the change in the electronic charge distribution, which is equilibrated with the excited-state dipole moment and polarizability.

To calculate solvation energies, the gas-phase values for the ground- and excited-state electrostatic properties need to be used in eq 8. These values are obtained from the B3LYP and MNDO−PSDCI calculations reported in ref 16. Therefore, the values used for μ_g and μ_e are 6 and 8 D, respectively, and the change in dipole moment is presumed to lie along the long axis of peridinin, *x*, as in a linear polyene. The $\bar{\alpha}_g$ value of 127 Å^3 used here[39] is separable into a 52 Å^3 contribution from the π-system and 75 Å^3 from the σ-system.[39,40] Therefore, an $\bar{\alpha}_e$ of 306 Å^3 is obtained from the 179 Å^3 $\overline{\Delta\alpha}_{el}$ reported in ref 16. The solvation energies for the *gas-phase* electronic transition energies are calculated in *n*-hexane, cyclohexane, MeTHF, tetrahydrofuran (THF), benzonitrile, and acetonitrile. Halogenated and hydrogen-bond-donating solvents were excluded to conserve uniform variability in the environment. As there are no gas-phase transition energies reported for peridinin in the literature, the calculated solvation energies are compared to experimental values relative to *n*-hexane ($h\Delta\nu_{calc}$ in Table 2), and not to the absolute energies. The solvent shifts are first calculated with the nonsolvated values reported in ref 16, where the ground-state properties are obtained from DFT calculations using a 6-31G(d) basis set, and the excited-state properties from MNDO−PSDCI calculations. The $\Delta\mu$ in this case is 2D.[16] The solvent shifts are then recalculated incorporating the experimental result for $\Delta\mu$ of 22 D. A corresponding gas-phase value of 18 D is extrapolated from 22 D by assuming a cavity field enhancement of 30% in MeTHF.

The solvation shifts in MeTHF and EG glasses have not been calculated as it is presumed to result from specific solvent−solute interactions that cannot be described using a dielectric continuum. When the temperature is "instantaneously" lowered to 77 K, it is presumed that the solute and solvent molecules are frozen in the ground-state configuration present at room temperature, thus preventing the solvent dipoles from equilibrating and properly aligning themselves around the solute dipoles. Furthermore, the change in the dielectric properties on glass formation, particularly in MeTHF where the index of refraction increases from 1.4 to 1.8 and ϵ_0 from 4 to 19,[27] would have to take into account additional solvent/solute interactions at a microscopic level to model these solvent shifts.

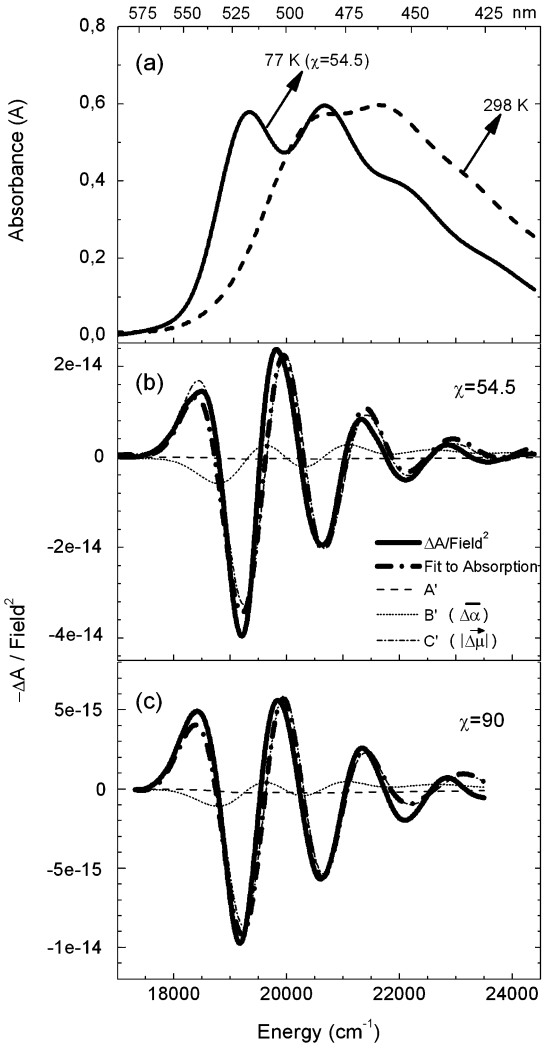

Figure 1. The absorption spectra of peridinin in MeTHF are shown in panel a at room temperature (dashed line) and at 77 K (solid line). The Stark spectrum (dark-solid line) and fit (dark-dot−dashed line) are shown in panel b at $\chi = 54.7°$, and in panel c at $\chi = 90°$. Also shown are the contributions of the first (A′ in light-dashed lines), second (B′ in light-dotted lines), and third (C′ in light-dot−dashed lines) terms in eq 1, to the fits in panels b and c. The *y*-axis units for the Stark spectra, which have been normalized by the square of the applied field, are in $(cm/V)^2$.

Results

Electronic Properties in MeTHF. The experimental absorption and Stark spectra of peridinin in MeTHF are shown in Figure 1. In panel a are the absorption spectra at room temperature (dashed line) and at 77 K (solid line). When the temperature is lowered, the absorption maximum red shifts by ~1000 cm^{-1} from 21 480 cm^{-1} (465.5 nm). In addition, the increase in resolution of the absorption spectrum reveals a

second peak at 19 340 cm^{-1} (517 nm), which was discernible as a shoulder (~482.5 nm) at room temperature. A more precise energetic origin for these bands is obtained by fitting the absorption spectrum to a sum of Gaussians centered at 18 000, 19 275, 20 590, 21 930, and 23 600 cm^{-1} at 77 K and at 19 030, 20 210, 21 550, and 23 070 cm^{-1} at room temperature. The Gaussians at 18 000 cm^{-1} (77 K) and at 19 030 cm^{-1} (room temperature) are less than a tenth the intensity of the others and are used merely to reproduce the absorption line shape at the red edge, and need not be included to get a good fit to the Stark signal. More importantly, the fit to Gaussians provides us with information not directly discernible from the absorption spectra. For example, the second and third Gaussians correspond to the shoulder and maximum, respectively, of the absorption spectra and actually exhibit uniform shifts of ~950 cm^{-1} when the temperature is lowered. Also, the fit of the absorption spectra in MeTHF (77 K) to Gaussians shows a vibronic progression of ~1300 cm^{-1} followed by a 1600−1700 cm^{-1} progression, similar to that reported in ref 12.

The experimental Stark spectra at 77 K (dark-solid lines) at $\chi = 54.7°$ and 90° with their respective fits (dark dot−dash lines) are shown in panels b and c, respectively. Along with the fits, in panels b and c are shown the three components of the fit. They are the weighted components of $A(\tilde{\nu})$ (light dashed line as A′) and the first (light dotted line as B′) and second (light dot−dash line as C′) derivatives of $A(\tilde{\nu})$, corresponding to the first, second, and third terms in eq 1, respectively. The highly structured Stark spectra are fit well to eq 1 across the entire absorption manifold, and the electro-optical parameters extracted from the fits may therefore be considered quite accurate. The second-derivative component, attributable to the change in dipole moment ($|\Delta\vec{\mu}|$), is the principal component of the Stark signal, whereas the first-derivative component, attributable to the change in the electronic polarizability, is comparatively much smaller for both $\chi = 54.7°$ and 90°. Indeed, the fits are quite similar to the second derivative of the absorption spectrum (compare dark and light dot−dash lines in Figure 1b,c) from which is derived a $|\Delta\vec{\mu}|$ value of 22 ± 3 D, and the ratio of $|\hat{m}\cdot\Delta\vec{\mu}|/|\Delta\vec{\mu}|$ yields a value of 0.98 ± 0.13 (Table 1) and a mean value of 11° between $|\Delta\vec{\mu}|$ and $\hat{m}$, the unit vector in the direction of the transition moment. The values of $\overline{\Delta\alpha}^{Stark}$ and $\Delta\alpha_m^{Stark}$ from $b_{54.7}$ and b_{90} are, respectively, −260 ± 170 and −900 ± 300 $Å^3$ and contain contributions from the transition-moment polarizability, A_{ij} (eq 3).

Electronic Properties in EG. The absorption and Stark spectra of peridinin in EG are shown in Figure 2. The absorption spectrum at room temperature in EG (dark-dashed line in Figure 2a) is broad and unstructured compared to that in MeTHF. Lowering the temperature to 77 K does not significantly increase the resolution of the absorption spectrum (dark-solid line in Figure 2a) beyond the shoulder that is revealed at ~19 400 cm^{-1} (515 nm). In addition, the absorption maximum merely red shifts by 10−20 cm^{-1}. The Stark spectrum at 77 K (dark-solid line) and fit (dark-dot−dash line) at $\chi = 54.7°$ are shown in Figure 2b and c, using two different fitting procedures (see Materials and Methods). In Figure 2b, the Stark spectrum is fit to a single set of electro-optical parameters derived from the derivatives of the absorption line shape. Although this fit to the Stark spectrum, in contrast to MeTHF, is poor in EG, the magnitude and general shape of the Stark signal is nevertheless reproduced. Therefore, the electrostatic properties extracted from this fit and reported in Table 1 can be used as a rough estimate for the change in dipolar properties undergone by peridinin, when excited within the absorption manifold in EG. The second-

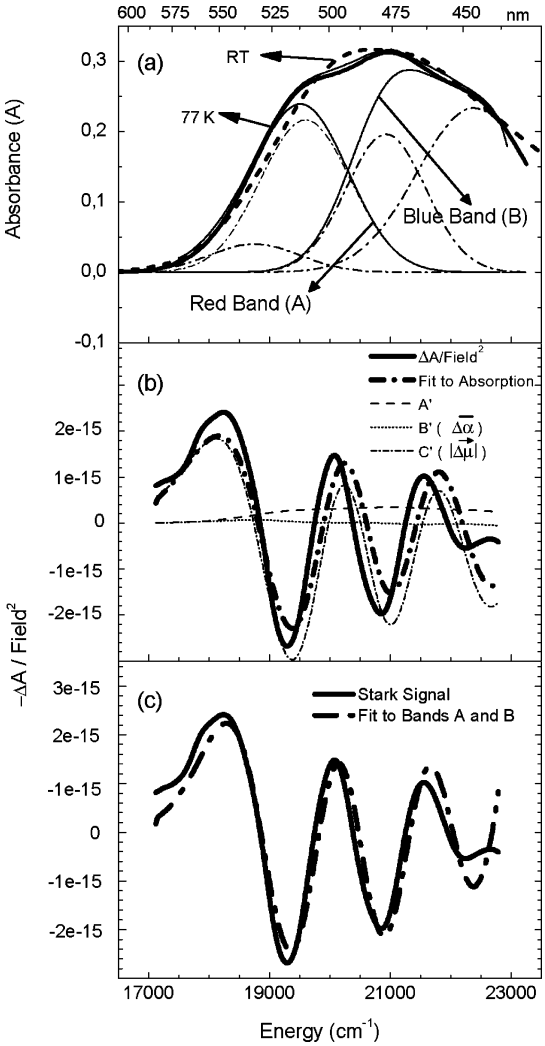

Figure 2. The absorption spectra of peridinin in EG are shown in panel a at room temperature (dark-dashed line) and at 77 K in EG glass (dark-solid line). The sum of bands A and B (light-solid line) is nearly indistinguishable from the 77 K absorption spectrum. The Stark spectrum (dark-solid line) and the fit (dark-dot−dashed line), at $\chi = 54.7°$, are shown in panel b to the absorption line shape, and in panel c to the derivatives of bands A and B (see Materials and Methods). Also shown in panel b are the contributions of the first (A′ in light-dashed lines), second (B′ in light-dotted lines), and third (C′ in light-dot−dashed lines) terms in eq 1 to the fit to the absorption line shape. The *y*-axis units for the Stark spectra, which have been normalized by the square of the applied field, are in $(cm/V)^2$.

derivative component (light-dot−dash line in Figure 2b), the primary source of the field-induced change in the absorption, as in MeTHF, yields a $|\Delta\vec{\mu}|$ of 27 D. The smaller contribution from the first-derivative component yields a −125 $Å^3$ $\overline{\Delta\alpha}^{Stark}$.

As previously described,[36] the poor quality fit to the Stark spectrum is indicative of regions within the absorption manifold possessing differing electronic properties and was therefore analyzed with two (or more) sets of variable electro-optical parameters in different regions of the spectrum. In EG, a minimum of two bands, comprising six independent variables (two sets of a_χ, b_χ, and c_χ), suffice to produce a good fit to the Stark spectrum of peridinin. These bands, A and B (Figure 2a), are each composed of two Gaussians (light-dot−dash lines). The choice of summing Gaussians 1 and 2 and Gaussians 3 and 4 into bands A and B, respectively, was motivated by the asymmetric regions in the fit to the Stark spectrum: below 19 000 cm^{-1} where the fit is smaller than the Stark signal (band

A), and between 19 000 and 22 500 cm^{-1} where the fit is shifted with respect to the Stark signal (band B). Indeed, the fit to the derivatives of bands A and B is markedly improved by increasing the free fitting parameters from three to six (Figure 2c). However, the lack of structure in the absorption spectrum makes it difficult to deconvolute the absorption spectrum into two bands for which we can obtain unique and accurate electro-optical parameters. The parameters obtained from this fit (Figure 2c) yield $|\Delta\vec{\mu}|$'s of 22 ± 5 D and 33 ± 8 D for band B and band A, respectively. The $\overline{\Delta\alpha}^{Stark}$ values from this fit are on the order of −2000 and −3000 $Å^3$, which are excessively large even if a contribution from the transition moment polarizability is present.[34,36] Despite the low precision in these values, we may infer that red edge (band A) excitation produces a more polar state than excitation at the blue edge, that is, the $|\Delta\vec{\mu}|$ for band A is larger than that for band B, consistent with the larger Stark signal evident at the red edge. The magnitude of $|\Delta\vec{\mu}|$ associated with absorption at higher energy in EG (band B) is now more similar to that obtained for peridinin in MeTHF.

The possibility that the species (or state) that gives rise to band A in EG may also be present in MeTHF was investigated by extracting the electro-optical properties of the red-most Gaussian, centered at 18 000 cm^{-1}. Separating this band and fitting it, as we do for EG, yields $|\Delta\vec{\mu}|$ values much larger than those for the main band. Since the intensity of this Gaussian is less than a tenth of the main absorption, the presence of such a band with stronger CT character must be marginal in MeTHF. Moreover, the LLSQ fit consistently produces an unstable solution for the parameters of this band at its red edge, due to its low intensity and its strong overlap with the adjacent Gaussian, and the results are therefore even less reliable than that for EG.

Solvent Shift Analysis. The estimation of the shift of the absorption maximum of peridinin in solvents of varying polarity is reported in Table 2, both within a spherical and an ellipsoidal solute cavity. Using a 2 D $\Delta\mu$ yields solvent shifts, $h\Delta\nu_{calc}$, that are an order of magnitude smaller than experiment with the spherical cavity yielding particularly weak results. On the other hand, incorporating an 18 D $\Delta\mu$ in eq 8 produces solvent shifts that are significantly larger. Note that the spherical cavity still underestimates the solvent shifts in all solvents, except cyclohexane, and it is only within an ellipsoidal cavity that the solvent shifts are similar to the experimental values (Table 2).[41]

Discussion

The most striking result obtained from the Stark experiments is that peridinin undergoes a large change in dipole moment on photon absorption, which has not been predicted nor envisioned previously for the $S_0 \rightarrow S_2$ transition. This finding can be integrated with other experimental observations and may indeed be necessary to understand the excited-state reactivity of peridinin.

The Origin of the Electronic Properties Measured in MeTHF versus EG. One of the implications of the large dipole moment that we have uncovered for the Franck−Condon region of the PES, being ≥22 D in MeTHF, is the possible influence from the ICT state on the properties of S_2, particularly in light of the much larger $\Delta\mu$ calculated for the $S_0 \rightarrow S_1$ (8 D) transition versus $S_0 \rightarrow S_2$ (2 D).[16] In fact, the meticulous analysis of the two-photon absorption and emission experiments, in conjunction with their MNDO−PSDCI calculations, lead Shima et al. to conclude that S_1 is itself the ICT state, which moreover strongly interacts with S_2.[16] The latter is evident in the two-photon absorption to the upper-vibronic levels of the $2^1A_g{}^{*-}$-like state, S_1, which shows that the transition moment between the one-photon allowed (S_2) and forbidden (S_1) states is large. Indeed, considerable mixing between S_1 and S_2 is also evident from the singly- and doubly excited configurations shared between the two states. Therefore, taking experimental and theoretical predictions into account, the effect of coupling between S_2 and the polar S_1/ICT state(s) should be manifested in the Stark spectra, presumably at the red edge where the S_1/ICT state would most affect the excited-state PES in the Franck−Condon region and result in a larger response to the applied field. However, the good fit of the Stark spectrum to the absorption line shape in MeTHF (Figure 1b) shows that the absorption of a photon both at high and at low energy results in the same changes in polarizability and dipole moment. This result suggests no influence of a lower energy ICT state on the $S_0 \rightarrow S_2$ transition in MeTHF, at least to the extent that S_2 does not borrow CT character from S_1/ICT. The homogeneous Stark spectra may nevertheless be reconciled, in the event of mixing between S_1 and S_2, if a comparatively nonpolar S_1 gains CT character by mixing with S_2. The Stark spectrum in this case would be dominated by the response of S_2 to the external field.

An interesting suggestion is that S_2 could be the ICT state itself, or rather that the ICT state could correspond to the relaxed S_2 state. The validity of the latter suggestion may be assessed by estimating the reorganization free energy (ΔG_{or}), half of which should correspond to the (solvent) equilibrated energy of S_2.[37] The values for $^1/_2\Delta G_{or}$ within an ellipsoidal cavity are found to be ∼800 cm^{-1} in, for example, acetonitrile and benzonitrile. The bottom of the S_2 potential well is then much higher than the S_1 state, which is between 2000 and 4000 cm^{-1} lower in energy.[12,17] However, the sub-100 fs decay of S_2 into ICT[17,19] does not preclude the possibility that the ICT state is the equilibrated S_2 state, which then decays into S_1 in a few picoseconds.[17,19] The decay into S_1 from ICT is presumed to be controlled by a solvent polarity dependent barrier.[22] Thus, the S_2, ICT, and S_1 states could be intimately linked via a structural coordinate;[12,17,19] a proposition that will be explored further for interpreting the results obtained in EG. Ultimately, these states would be affected by environmental conditions in ways that could control the functionality of peridinin within the PCP.

The improvement in the fit to the Stark spectrum in EG using two bands (Figure 2c) indicates that the absorption band of peridinin is effectively composed of (at least) two electronic/vibronic states corresponding to bands A and B. This occurrence of two energetic regions with disparate electronic properties is supported by transient absorption (TA) spectra of peridinin in EG at room temperature, where the rise and decay times of the ICT state when probed at 950 nm exhibit different time scales following excitation at 550 nm (18 200 cm^{-1}) or 425 nm (23 500 cm^{-1}).[17] Similarly, the Stark spectrum in EG indicates that excitation within bands A and B initially populates different electronic/vibronic states. In contrast, in polar environments such as acetonitrile, excitation-wavelength-dependent dynamics are not observed in the TA spectra[17] similar to the Stark spectrum in MeTHF that shows no wavelength-dependent change in the electronic properties.

The question therefore remains regarding the origin of bands A and B, separated by ∼2000 cm^{-1} (Figure 2a). They could be potentially assigned to either (a) one dominant peridinin conformer where A and B represent two distinct electronic/vibronic states or (b) different ground-state conformers. Without choosing either option a or option b, the case may be made for band B, at higher energy, to be similar in origin to the absorption

in MeTHF, which both have $|\Delta\vec{\mu}|$'s on the order of 22 D. The origin and identification of band A in EG is however contentious and could be rationalized either by option a, as suggested by "pump−dump−probe" measurements in methanol,[19] or by option b, as suggested by other TA measurements in EG.[17] One possibility in option a is that band A is itself the ICT state, given that its dipole moment is 10−20 D larger than that of band B. However, excitation at 550 nm in EG still produces a TA spectrum that decays into a distinct ICT state with a faster and less pronounced rise of the ICT band than when excited at 425 nm,[17] which lies within band B. It is unlikely that, if band A corresponds to the unrelaxed part of the ICT state, it is manifested in the Stark spectrum in EG but not in MeTHF, where a similar energy envelope between 17 500 and 23 000 cm^{-1} is probed. On the other hand, option b where the presence of ground-state conformers is invoked could account for the asymmetry in the Stark spectrum uniquely present in EG. Moreover, the ICT state is linked to a geometry distortion,[12,17,19] which can be promoted in a hydrogen-bonding environment such as that provided by EG. Indeed, those peridinins that adopt a conformation in the ground state similar to that of the ICT state could more easily overcome the barrier to a geometry distortion in the excited state. The TA spectra of peridinin arising from excitation at 550 nm in EG could well arise from such a species.[17] Notably, the Stark signal of band A in EG is rather similar at the red edge of the carotenoid absorption in the native protein environment of PCP (unpublished). These red-absorbing carotenoids are suggested to have a twisted, non-cis geometry and, moreover, play an important role in energy-transfer dynamics.[11,16,20,42]

The Impact of Photoinduced Charge Transfer. The 22 D $|\Delta\vec{\mu}|$ measured for the $S_0 \rightarrow S_2$ transition of peridinin is clearly indicative of significant redistribution of electronic charge in the Franck−Condon region. An increase in the dipole moment on excitation, $\mu_e > \mu_g$, and therefore a positive $|\Delta\vec{\mu}|$, may be inferred from the decrease in energy of the absorption maximum with increasing solvent polarity (Table 2). Moreover, $|\Delta\vec{\mu}|$ is nearly parallel to $\hat{m}$, which is typically found in linear all-trans polyenes,[43] therefore confirming the presence of a linear conformer of peridinin in MeTHF at 77 K. The angle between $|\Delta\vec{\mu}|$ and $\hat{m}$, although quite different from the 46° predicted by MNDO−PSDCI calculations, is in fact in better agreement with the experimental polarization ratio for two-photon absorptivity to S_2.[16]

The 22 D $|\Delta\vec{\mu}|$ in this all-trans type peridinin present in MeTHF is equivalent to one *full* electron moving over ∼4.5 Å on excitation.[44] Inspection of the molecular structure (Scheme 1) indicates the most likely electron donor and acceptor to be the allene and lactone group, respectively. To produce a 22 D $|\Delta\vec{\mu}|$ between these two groups, more than 10 Å apart, partial electronic charge, rather than one full electron, would be transferred on photon absorption. Nevertheless, the >22 D dipole moment of S_2 would be expected to have an impact, particularly in the protein, where the large μ_e could bring about efficient dipolar coupling to Chl-*a* in PCP, to account for the >20% energy transfer directly from S_2.[8,9] An indirect, but relevant, effect is envisioned via the facilitation of the formation of the ICT state, from which up to 80% of the energy transfer to Chl-*a* occurs,[8,9] and will be discussed later.

More information about the interaction between excited states could be obtained from $\overline{\Delta\alpha_{el}}$, where strong coupling between S_2 and S_1 may be manifested as a very small or even negative $\overline{\Delta\alpha_{el}}$.[45] However, the experimental $\overline{\Delta\alpha}^{Stark}$ of −260 $Å^3$ (Table 1) is physically unrealistic if assigned entirely to $\overline{\Delta\alpha_{el}}$, since the $\bar{\alpha}_g$ of 127 $Å^3$ would imply that $\bar{\alpha}_e$ is negative. Therefore, the likely contribution of A_{ij} to $\overline{\Delta\alpha}^{Stark}$ (eq 3) and to $\Delta\alpha_m^{Stark}$ (eq 5) prevents us from commenting on the accuracy of the +179 $Å^3$ calculated for $\overline{\Delta\alpha_{el}}$, except to observe that it is usually more difficult to calculate excited-state properties, more so for $\bar{\alpha}_e$ than μ_e. To arrive at a more accurate value for $\overline{\Delta\alpha_{el}}$, the A_{ij} value would need to be ascertained. Although the value of A_{ij} cannot be directly obtained from $a_{54.7}$, unless B_{ijj} is presumed negligible, this term is negative in both MeTHF and EG. The anomalously large negative values obtained for $\overline{\Delta\alpha}^{Stark}$ and $\Delta\alpha_m^{Stark}$ could thus be caused in part by the A_{ij} term. It is worthwhile to note that other (large) polarizability differences reported in the literature may also contain contributions from A_{ij},[36] particularly if $\overline{\Delta\alpha}^{Stark}$ is equated to $\overline{\Delta\alpha_{el}}$.

Certainly, the large change in dipole moment measured here for peridinin challenges previous estimations for $\Delta\mu$ associated with the strongly allowed $S_0 \rightarrow S_2$ transition.[12,16,17] Nevertheless, corroboration of our experimental results is found in the solvent shift analysis. Indeed, a gas-phase $\Delta\mu$ of at least 18 D is necessary to reproduce the experimental values[10] (compare $h\Delta\nu_{calc}$ and $h\Delta\nu^{exp}$ in Table 2). Clearly, these shifts are underestimated with a 2 D $\Delta\mu$. We note that the underestimation of $h\Delta\nu_{calc}$ in the ellipsoidal cavity by ∼100−200 cm^{-1} in acetonitrile and benzonitrile does not arise because $\alpha_g R_{or}$ is assumed to be ≪1 but probably because the perturbation approach used to formulate eq 8 is inadequate when there is strong solvent-induced enhancement of the dipole moments.[46]

Comparison to Electronic-Structure Calculations. The only $\Delta\mu$ value reported in the literature for the $S_0 \rightarrow S_2$ transition from MNDO−PSDCI calculations[16] is a factor of 10 smaller than that measured here. In general, estimates of ground-state properties are more likely to be accurate where the PES is often straightforward to model, whereas excited-state properties are more difficult to evaluate, where a manifold of excited electronic states, and particularly those energetically close to S_2, would need to be accurately modeled.[21,43] The agreement between MNDO−PSDCI[16] and TDDFT[14] for the ground-state properties ($\mu_g \approx 6$ D) further attests to the robustness of ground-state calculations. The excited-state electrostatic properties obtained by the above two methods appear, however, to be quite different. MNDO−PSDCI predicts a μ_e of ∼8 D for S_2 yielding a 2 D $\Delta\mu$ for the $S_0 \rightarrow S_2$ transition.[16] Although the excited-state dipole moments were not explicitly reported for the TDDFT calculations,[14] a 50 D μ_e was "back-calculated" for S_2 from the equation used to estimate the stabilization energies, given in the same article, for *n*-hexane and acetonitrile.[14] This 50 D value for μ_e is likely to be an overestimation, because the stabilization energy difference of 4000 cm^{-1} reported in ref 14 is nearly a factor of 4 greater than experiment. Although the electrostatic properties of S_2 obtained from calculations are in disagreement with our experimental findings, they nevertheless yield reasonably accurate electronic transition energies, particularly notable for the $S_0 \rightarrow S_1$ transition. Therefore, given the accuracy of the transition energies, indeed an important criterion for evaluating the reliability of calculations, it is still possible to obtain qualitatively useful information from them. The results from the MNDO−PSDCI calculations[16] will primarily be used to provide additional insights below.

One important contribution from such calculations is a description of the molecular orbitals that contribute to the electronic transition, which can be used to determine the direction of electron motion, and in particular, the electron-donor and -acceptor moieties. The MNDO−PSDCI calculations

show that the $S_0 \rightarrow S_2$ transition is ~70% HOMO−LUMO, although including other promotions, in total 80% of the transition originates in the HOMO and terminates in the LUMO. They are found to be delocalized over the polyene backbone in the ground state (HOMO) and localized toward the lactone end of the polyene chain in the excited state (LUMO). The allene and lactone groups, previously suggested to be the most likely electron donor and acceptor, respectively (see above), are indeed shown to lose and gain electron-charge density, respectively, on excitation.[47] Therefore, from these molecular orbital representations, the 22 D $|\Delta\vec{\mu}|$ would result from ~40% of an electron transferred over a maximal distance of 10 Å from the allene to the lactone (see Scheme 1).

Further insight into the nature of the distortion, previously suggested to be associated with the ICT state, can be obtained by examination of the excited-state wave function of S_2. The antibonding breaks that accompany a change in the LUMO wave function, that is, nodes (see dark-dashed lines in Scheme 1), are probably the most flexible points, which when located between two atoms identify the bonds most likely to be distorted or bent in the excited state. Interestingly, one of these nodes is located on the carbonyl bond (in the lactone ring), which is associated with the formation of the ICT state.[12,19,48] The location of these nodes suggests a possible distortion comprising a concerted action between the carbonyl group and the lactone ring to generate the ICT state. Note that the formation of the node(s) would be linked to charge transfer to the carbonyl oxygen on photon absorption.

Finally, although our study has focused on peridinin, it is possible that in addition to spheroidenone,[49] other carotenoids containing a carbonyl group[32,48,50] will be shown by Stark spectroscopy to have a large dipole on excitation to S_2. In polar solvents, both fucoxanthin and siphonaxanthin form a low-lying CT state after excitation to S_2 ($1^1B_u{}^{*+}$).[3] In diatom thylakoids, fucoxanthin also shows anomalous two-photon excitation reminiscent of peridinin in solution and in PCP.[50]

Conclusions

The Stark spectra of peridinin reveal that peridinin undergoes photoinduced charge transfer, both in polar (MeTHF) and in protic polar (EG) environments, where $|\Delta\vec{\mu}|$'s on the order of 20−30 D for the $S_0 \rightarrow S_2$ transition have been measured. The unexpectedly large dipole moment found for S_2 is corroborated by the calculated shift of the absorption band of peridinin as a function of solvent polarity. The CT character of the S_2 state is postulated to be necessary to generate the previously identified ICT state, probably via a geometry distortion that stabilizes the initially formed charge-separated species. Furthermore, the large dipole moment would allow for strong dipolar coupling and would account for direct energy transfer from S_2 of peridinin to Chl-*a* in PCP. The highly polar nature of S_2 found in our experiments suggests that current theoretical models need to be further refined to capture the true electrostatic properties of the peridinin S_2 state.

Acknowledgment. L.P., E.P., and R.v.G. would like to acknowledge the Foundation for Fundamental Research on Matter (FOM) of The Netherlands and the Dutch Science Organization (NWO) for financial support. R.G.H. was supported by the Australian Research Council (Grant AO0000264). L.P. is grateful to Prof. Robert Birge for the polarizability calculations and insightful comments.

References and Notes

(1) Frank, H. A.; Cogdell, R. J. *Carotenoids in Photosynthesis*; Chapman and Hall: London, 1993.
(2) Mimuro, M.; Nagashima, U.; Takaichi, S.; Nishimura, Y.; Yamazaki, I.; Katoh, T. *Biochim. Biophys. Acta* **1992**, *1098*, 271.
(3) Polivka, T.; Sundström, V. *Chem. Rev.* **2004**, *104*, 2021.
(4) Marder, S. R.; Torruellas, W. E.; Blanchard-Desce, M.; Ricci, V.; Stegeman, G. I.; Gilmour, S.; Bredas, J.-L.; Li, J.; Bublitz, G. U.; Boxer, S. G. *Science* **1997**, *276*, 1233.
(5) *Organic Molecules for nonlinear Optics and Photonics*; Messier, J., Kajzar, F., Prasad, P., Eds.; Kluwer: Dordrecht, The Netherlands, 1991; Vol. 194.
(6) Yoon, H. S.; Hackett, J. D.; Bhattacharya, D. *Proc. Natl. Acad. Sci. U.S.A.* **2002**, *99*, 11724.
(7) Bautista, A.; Hiller, R. G.; Sharples, F. P.; Gosztola, D.; Wasielewski, M. R.; Frank, H. A. *J. Phys. Chem. A* **1999**, *103*, 2267.
(8) Krueger, B. P.; Lampoura, S. S.; van Stokkum, I. H. M.; Papagiannakis, E.; Salverda, J. M.; Gradinaru, C. C.; Rutkauskas, D.; Hiller, R. G.; van Grondelle, R. *Biophys. J.* **2001**, *80*, 2843.
(9) Zigmantas, D.; Hiller, R. G.; Sundström, V.; Polvka, T. *Proc. Natl. Acad. Sci. U.S.A.* **2002**, *99*, 16760.
(10) Bautista, J. A.; Connors, R. E.; Raju, B. B.; Hiller, R. G.; Sharples, F. P.; Gosztola, D.; Wasielewski, M. R.; Frank, H. A. *J. Phys. Chem. B* **1999**, *103*, 8751.
(11) Carbonera, D.; Giacometti, G.; Segre, U.; Hofmann, E.; Hiller, R. G. *J. Phys. Chem. B* **1999**, *103*, 6349.
(12) Frank, H. A.; Bautista, J. A.; Josue, J.; Pendon, Z.; Hiller, R. G.; Sharples, F. P.; Gosztola, D.; Wasielewski, M. R. *J. Phys. Chem. B* **2000**, *104*, 4569.
(13) Ilagan, R. P.; Shima, S.; Melkozernov, A.; Lin, S.; Blankenship, R. E.; Sharples, F. P.; Hiller, R. G.; Birge, R. R.; Frank, H. A. *Biochemistry* **2004**, *43*, 1478.
(14) Vaswani, H. M.; Hsu, C.-P.; Head-Gordon, M.; Fleming, G. R. *J. Phys. Chem. B* **2003**, *107*, 7940.
(15) Linden, P. A.; Zimmerman, J.; Brixner, T.; Holt, N. E.; Vaswani, H. M.; Hiller, R. G.; Fleming, G. R. *J. Phys. Chem. B* **2004**, *108*, 10340.
(16) Shima, S.; Ilagan, R. P.; Gillespie, N.; Sommer, B. J.; Hiller, R. G.; Sharples, F. P.; Frank, H. A.; Birge, R. R. *J. Phys. Chem. A* **2003**, *107*, 8052.
(17) Zigmantas, D.; Hiller, R. G.; Yartsev, A.; Sundström, V.; Polivka, T. *J. Phys. Chem. B* **2003**, *107*, 5339.
(18) Zimmerman, J.; Linden, P. A.; Vaswani, H. M.; Hiller, R. G.; Fleming, G. R. *J. Phys. Chem. B* **2002**, *106*, 9418.
(19) Papagiannakis, E.; Larsen, D. S.; Stokkum, I. H. M.; Vengris, M.; Hiller, R. G.; van Grondelle, R. *Biochemistry* **2004**, *43*, 15303.
(20) Kleima, F. J.; Hofmann, E.; Gobets, B.; van Stokkum, I. H. M.; van Grondelle, R.; Diederichs, K.; van Amerongen, H. *Biophys. J.* **2000**, *78*, 344.
(21) Hudson, B.; Kohler, B. *J. Chem. Phys.* **1973**, *59*, 4984.
(22) Zigmantas, D.; Polivka, T.; Hiller, R. G.; Yartsev, A.; Sundström, V. *J. Phys. Chem. A* **2001**, *105*, 10296.
(23) Liptay, W. Dipole moments and polarizabilities of molecules in excited states. In *Excited States*; Lim, E. C., Ed.; Academic Press: New York, 1974; Vol. Vol 1, p 129.
(24) Liptay, W.; Becker, J.; Wehning, D.; Lang, W.; Burkhard, O. *Z. Naturforsch.* **1982**, *37a*, 1396.
(25) Note that the term "dipole moment" is always used in this manuscript for the permanent dipole moment and not the transition dipole moment.
(26) Martinson, T. A.; Plumley, F. G. *Anal. Biochem.* **1995**, *228*, 123.
(27) Bublitz, G. U.; Boxer, S. G. *J. Am. Chem. Soc.* **1998**, *120*, 3988.
(28) Premvardhan, L. L.; van der Horst, M. A.; Hellingwerf, K. J.; van Grondelle, R. *Biophys. J.* **2003**, *84*, 3226.
(29) Premvardhan, L. L.; Wachsmann-Hogiu, S.; Peteanu, L. A.; Yaron, D. J.; Wang, P. C.; Wang, W.; MacDiarmid, A. G. *J. Chem. Phys.* **2001**, *115*, 3975.
(30) Bublitz, G. U.; Boxer, S. G. *Annu. Rev. Phys. Chem.* **1997**, *48*, 213.
(31) Krawczyk, S.; Olszowka, D. *Chem. Phys.* **2001**, *265*, 335.
(32) Krawczyk, S.; Britton, G. *Biochim. Biophys. Acta* **2001**, *1544*, 301.
(33) Locknar, S. A.; Peteanu, L. A. *J. Phys. Chem. B* **1997**, *102*, 4240.
(34) Reimers, J. R.; Hush, N. S. *J. Phys. Chem.* **1991**, *95*, 9773.
(35) Chowdhury, A.; Locknar, S. A.; Premvardhan, L. L.; Peteanu, L. A. *J. Phys. Chem. A* **1999**, *103*, 9614.
(36) Premvardhan, L. L.; Peteanu, L. A. *J. Phys. Chem. A* **1999**, *103*, 7506.
(37) Böttcher, C. J. F. *Theory of Electric Polarisation*; Elsevier Publishing Co.: Amsterdam, 1952.
(38) Kim, H. J. *J. Chem. Phys.* **1996**, *105*, 6833.
(39) Birge, R. Personal communication, 2004.
(40) Martin, C. H.; Birge, R. R. *J. Phys. Chem. A* **1998**, *102*, 852.
(41) Using a α_g of 127 Å^3 and *a* of −120 Å^3 changes the values reported in Table 2 less than 10%.
(42) Damjanovic, A.; Ritz, T.; Schulten, K. *Biophys. J.* **2000**, *79*, 1695.
(43) Locknar, S. A.; Peteanu, L. A.; Shuai, Z. *J. Phys. Chem. A* **1999**, *103*, 2197.

(44) The transfer of one electron over 1 Å amounts to a 4.8 D dipole moment in vacuo.

(45) In the sum-over-states (SOS) expression, the polarizability of state i, α_i, is proportional to the square of the transition moment and inversely proportional to the energy gap, ΔE, with respect to each state, f, in the entire electronic manifold ($\alpha_i = \sum_f |\langle f|\hat{m}_{fi}|i\rangle|^2/(E_f - E_i)$). The negative contributions to this summation arise from coupling to energetically close lower energy states.

(46) Kim, H. J.; Hynes, J. T. *J. Chem. Phys.* **1992**, *96*, 5088.

(47) In contrast to the implication of the ubiquitous steric bond between the allene and the polyene backbone, the fact that the allene is also conjugated indicates that it cannot be completely bent out of the plane of the polyene backbone.

(48) Zigmantas, D.; Hiller, R. G.; Sharples, F. P.; Sundström, V.; Polivka, T. *Phys. Chem. Chem. Phys.* **2004**, *6*, 3009.

(49) Gottfried, D. S.; Steffan, M. A.; Boxer, S. G. *Biochim. Biophys. Acta* **1991**, *1059*, 76.

(50) Shreve, A. P.; Trautman, J. K.; Owens, T. G.; Albrecht, C. Carotenoid to chlorophyll a singlet energy transfer: direct evidence for involvement of the carotenoid A state in an algal light harvesting system. In *Current Research in Photosynthesis*; Baltscheffski, M., Ed.; Kluwer Academic Publishers: Amsterdam, 1990; Vol. 2. p 293.